Proc. 7th Int. Conf. on Erosion by Liquid and Solid Impact

DYNAMICS OF VORTEX CAVITATION INVOLVED IN THE EROSION OF HYDRAULIC MACHINES

F. Avellan*, A. Karimi**
*Institut de Machines Hydrauliques et de Mécanique des Fluides
**Institut de Génie Atomique
Ecole Polytechnique Fédérale, 1015 - Lausanne (Switzerland)

ABSTRACT

In order to investigate the dynamics of the vortex cavitation, which is found to be responsible of the cavitation erosion in hydraulic machinery, a cavitation vortex generator (CVG) is used. By producing the cyclic growth and collapse of cavitation vortex, this device provides a good simulation of the realistic hydrodynamics situation corresponding to the travelling cavities downstream a fixed leading-edge cavity. The simultaneous use of the shock and the pressure time-history recordings and the high speed Cranz-Schardin visualizations allows us to describe the instantaneous cavity motion in the CVG test section. The most important result is the evidence of a strong spherical shock waves emission at the time of the cavitation vortex collapse, leading to overpressure of more than 10 kbar.

INTRODUCTION

Cavitation erosion of hydraulic machines is of great economical importance to the power generation industry. The problem of the cavitation erosion does not only affect the hydropower generation but also the whole power generation field. As far as hydropower is concerned, cavitation erosion prevents us from designing hydraulic turbines or high head storage pumps with a higher specific power or from setting these machines at a lower level in the plant. In the same way the availability to electric utilities of both nuclear and fossil power plants can be limited by trouble-shooting due to severe erosion of high energy pumps, such as boiler feed pumps or large circulating pumps of condenser cooling water. In both cases of hydraulic machines, considered as a main component or auxiliary components of the power generation system, the trend is to operate under cavitation condition mainly during off-design operation as long as the hydraulic performances are not affected by the cavitation extension over the runner. The erosion problem cannot be overcome by simply eliminating the cavitation, but should be considered as an acceptable risk. Then the problem arises concerning the prediction of the cavitation erosion. To solve this problem, the "Institut de Machines Hydrauliques et de Mécanique des Fluides" (IMHEF) decided on an interdisciplinary research program at EPFL, in collaboration with the "Institut de Génie Atomique" (IGA) and the Laboratoire de Mécanique Appliquée"(LMA).

For six years our research work has been concentrated on the study of the physical aspect of the cavitation erosion in hydraulic machinery. The use of the IMHEF universal hydraulic machine test loop (2) and the IMHEF new high-speed cavitation tunnel (3) allows us to identify the type of cavitation associated with the erosion of hydraulic machines. In both types, e.g. pumps and turbines, severe erosion of runners is associated with the presence of travelling cavitation vortices, see Figure 1, which collapse in high pressure regions of the runner. Morever, we found that the most studied cavitation, i.e. the travelling bubble cavitation does not occur frequently in industrial machines, and is rarely associated with erosion in the case of a good hydraulic blade design. The travelling cavities of industrial interest present an irregular three-dimensional U-shape, see Figure 2, which is far from the quasi-spherical shape of the travelling bubble cavitation. The travelling cavitation vortices are created downstream of a fixed leading-edge cavity by the flow acceleration

Fig. 1. Travelling cavitation vortices downstream the leading edge cavitation of a pump-turbine runner model in pump operation.

at the closure of the fixed cavity. According to the sketch presented in Figure 3, the stretching of the vorticity lines, by Kelvin- Helmholtz instabilities (4), produces a low pressure region in the core of the vortices where cavities can be found. These cavitation vortices are then convected by the mean-flow to the pressure recovery regions. Unlike the travelling bubble cavitation, for which cavity collapses can occur in the bulk flow depending of their random positions, the cavitation vortices sweep the blade-wall with their tips according to the Helmholtz theorem, and accordingly the cavity collapse should occur close to the blade wall producing severe damage of the material.

Fig. 2 Side view showing the 3-D U-shape of the travelling cavitation vortices in the case of a 2-D hydraulic blade profile in the new IMHEF high-speed cavitation tunnel.

Since a new hydrodynamic process of erosion was identified, two experimental approaches were chosen in both fluid mechanics and materials science. The first approach was to investigate a macroscopic erosive situation corresponding to one which can be observed in hydraulic machine. This is carried out with a two dimensional hydraulic blade profile of a 100 mm chord length in the IMHEF new high-speed cavitation tunnel, where we can reach velocity of up to 50 m/s. The second investigation path was to use a laboratory device where cavitation vortices could be isolated and studied. This device. called the cavitation vortex generator (CVG). was first developed by Lecoffre et al. (5), and thereafter improved by the authors to produce controlled and repeated cavitation vortex collapse on test specimens. In addition, the test section was changed to visualize cavitation vortex. A systematic comparison of the various cavitation erosion situations was already carried out by the authors (6) to see whether the CVG was able to produce the same cavitation erosion compared to the damages observed in hydraulic machinery. The aim of this paper is to describe the dynamics of the cavitation vortex observed in the CVG in order to explain the hydrodynamic process by which material damages are caused. First, we describe the CVG and the hydraulic operation of that device. Thereafter. the experimental set-up, involving the high-speed Cranz-Schardin camera and the pressure instrumentation, is detailed Finally the resulting visualizations related to the bulk pressure evolution in the CVG test section allow us to discuss the different stages of the complete cavity life cycle and to have an insight into the cavitation vortex collapse.

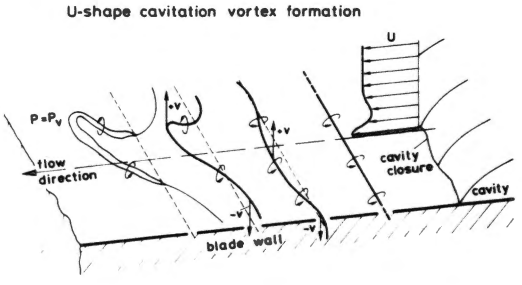

Fig. 3. Sketch of the U-shape cavitation vortices formation at a fixed cavity closure.

THE CAVITATION VORTEX GENERATOR

Hardware description. The cavitation vortex generator is a hydraulic closed loop consisting of a test section where erosion tests and visualization can be carried out, a rotating valve, a set of vessels and a circulating pump, see Figure 4.

The test section is made of a cylindrical chamber of 80 mm diameter and 20 mm width with a tangential inlet of 10 mm diameter. A 40 mm long truncated volume of a circular to a rectangular cross-section change, and a 24 mm diameter circular outlet are located on each side of the inlet chamber with the same axis, see Fig. 5

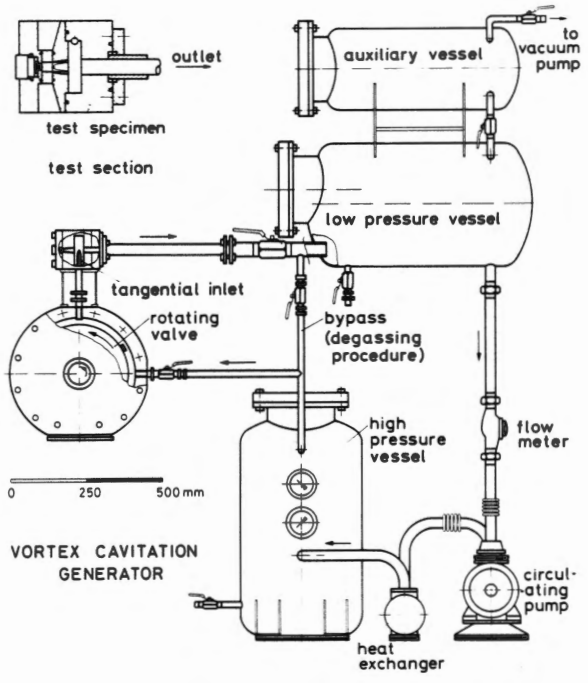

Fig. 4. Diagram of the cavitation vortex generator.

The rotating valve is made of a disk driven by a DC motor. The shutter which consists of a piece of a circular ring of a 159 mm outer radius and a 40 mm length, is fixed on the disk periphery, see Figure 6. The shutter radius is adjusted to allow, in a closed position, a 0.2 mm spacing with the end of the 8 mm diameter pipe which connects the valve to the test section. The valve velocity can be varied in the range of 0 to 1000 RPM. The multi-stage centrifugal pump is connected to the CVG circuit through two vessels of 60 liter unit volume.

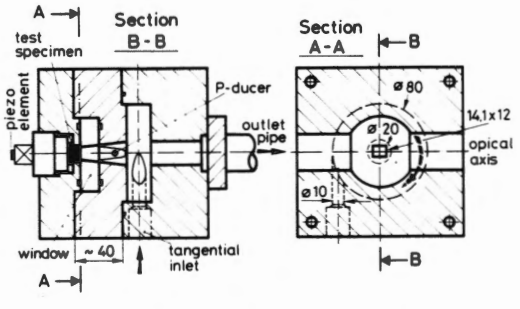

Fig. 5 Side and top viewsof the test section of the CVG (all the dimensions are in mm).

Due to the CVG head losses, the circulating pump gives a flow rate of up to 3 m^3/hour which corresponds to a total pressure of 9.5 bar. The flow rate can be adjusted by changing the pump speed. A heat-exchanger is installed at the pump outlet to keep the CVG water temperature constant at 19 °C.

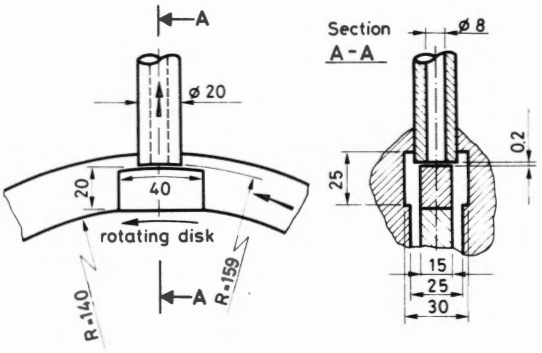

Fig. 6. Diagram of the shutter of the rotating valve (all the dimensions are in mm).

Operation of the CVG. The principle of the CVG is to produce, at each revolution of a rotating valve, a series of expansion-compression waves in order to promote cyclic growth and collapse of cavities in a vortex flow field.

During the open valve position, which is 96% of one valve-revolution, the tangential inlet flow induces a rotational motion in both the truncated volume of the test section and the outlet pipe. In the outlet pipe, an axial motion is combined with a vortex flow centered on the test section axis. According to the Helmholtz vortex law (7), the velocity line extends downstream to the vessel and upstream to an axisymmetric stagnation point at the end of the truncated volume where the test specimen is fitted. In the center part of the flow, the viscosity effect leads to a free vortex flow field with a solid body rotation core. This solid rotation provides a finite under-pressure difference between the bulk pressure and the center of the core, in contrast to the free vortex.

At the cut-off of the flow, the resulting water-hammer generates an expansion wave in the test section. Water-hammer transient calculations show that flow vaporization occurs already at the valve during the final stage of the flow cut-off, though the valve is not completely closed. However, depending on the wave transit times, 0.2 ms between the valve and the test section and 0.4 ms between the test section and the upstream vessel, the pressure in the test section is decreasing gradually, see Figure 7. The calculated case corresponds to a flow rate of 0.8 l/s and a valve rotation speed of 200 RPM. Since the rotational motion of the flow in the test section and the outlet pipe cannot be affected in a few milliseconds, the flow vaporization occurs in the vortex core. As long as the valve is closed, the cavitation extends into the central part of the

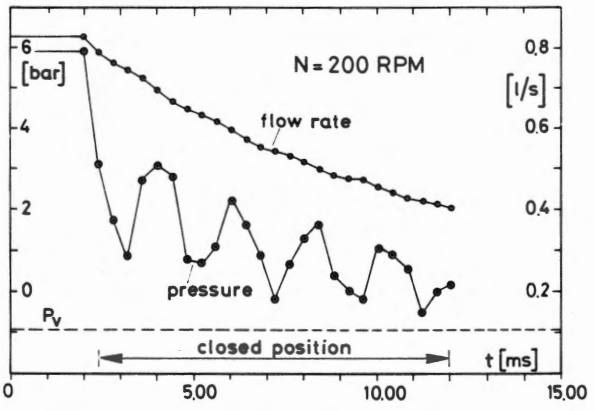

Fig. 7. Transient calculations of the pressure and the flow rate history in the test section during the flow cut-off.

test section. When the valve opens, the overpressure at the valve forces the cavity to collapse.

However. the cavitation vortices are directly controlled in the CVG by two operating parameters, e.g. the pump discharge and the valve rotation speed. The pump discharge value imposes the steady pressure distribution in the test section and the overpressure at the valve opening. The valve rotation speed,which obviously gives the duration of the closed valve position, limits the size of the cavity extension in the test section.

The operation remains efficient as long as the CVG circuit water is desaerated. The presence of dissolved gases leads to the growth of a steady gaseous cavity in the test section, even during the open position of the valve, and then prevents the CVG to operate efficiently. However, before each test, and at least every day, a special degassing procedure is carried out with a vacuum pump. The gas content of the water is monitored with an oxygen probe and kept lower than 1 ppm.

INSTRUMENTATION

High-speed camera. To visualize the transient phenomena involved in the CVG test section a high-speed shadowgraph system is used. This is achieved with a Cranz-Schardin camera. The Cranz-Schardin camera, which is an improved system based on an Institut of Saint Louis (West Germany) design (8), consists of a set of 16 spark-generators used as short-duration light sources, and 16 corresponding achromat objectives which provide 16 frames on the same 4" x 5" photographic plate placed at the back plane of the camera.

The position of the sparks corresponds to the focal plane of a first field lens of a 1600 mm focal length in order to obtain a parallel illumination of the test section. The camera objectives of a 380 mm focal length and a 11.8 diameter are located at the focal plane of a second field lens in order to provide shadow graph pictures on the image plane as shown in Figure 8. A rectangular mask is inserted in front of the CVG test section to avoid the interference of the images on the photographic plate.

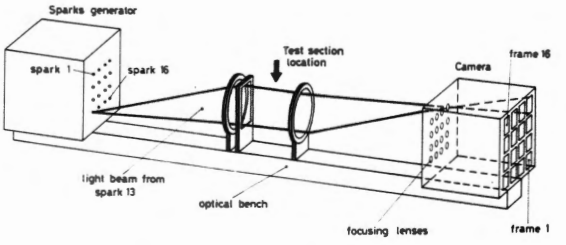

Fig. 8. Optical arrangement of the high-speed Cranz-Schardin camera.

As a part of the test section itself, a high-optical quality glass window is installed just in front of the test specimen. The window is made of bonded glass blocks of ground parallel faces, see Figure 9, and is coated on the external faces to overcome the light reflection.

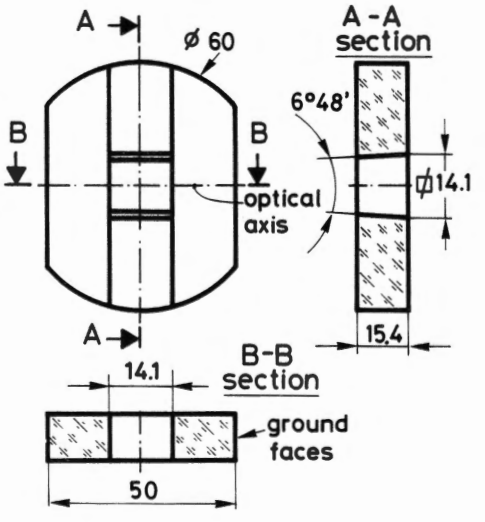

Fig. 9. Optical window of the test section (all the dimensions are in mm).

The sparks are generated by 2.4 J energy air-discharges through a 47 nF capacitor, charged at 10 kV, which results in flash lights of less than 300 ns. The discharges are triggered by an electronic time-unit which provides an adjustable spark rate of 1 KHz to 10 MHz with a constant time resolution of 50 ns between each trigger pulse.

Pressure instrumentation. To record the pressure evolution with respect to the cavitation development in the test section, and the rotating valve position, a pressure transducer is flush-mounted on the test section wall, see Figure 5. In order to have as short rise time as possible, we choose the 603B Kistler model which is a quartz pressure transducer of a 1 µs rise time, a 400 kHz natural frequency and a 0 to 200 bar pressure range. This model is acceleration compensated to overcome the external vibration perturbations. The charge signal is amplified and converted through a TA 3/D Vibrometer charge-amplifier with a 300 kHz band pass limit.

In addition, a PXE 41 Philips piezoelectric ceramic is placed at the end of the test specimen support in order to monitor the shocks and the vibrations on the test section.

All the signal outputs are indifferently stored and displayed on a transient recorder or an oscilloscope.

Each set of simultaneous signal records and visualization sequences is triggered by an adjustable delay from the start of the valve closing.

RESULTS

Cavity life cycle. The simultaneous recordings of the acceleration signal behind the test specimen, the pressure signal in the test section and the photograph sequence allow us to investigate the explosive growth and the collapse of the cavitation vortex in the CVG test section.

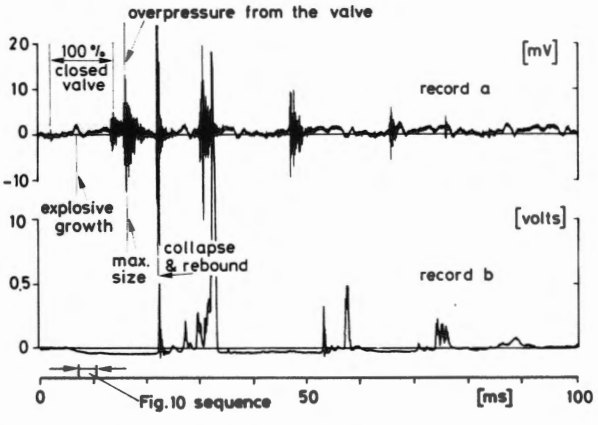

Fig. 10. Acceleration and pressure signals corresponding to the cavity life cycle. Recording a : piezoelement output. Recording b : p-dycer output. Nominal flow rate = 3 m^3/Hour, N = 200 RPM, time origin is taken at the start of the valve closing.

As it is shown in Figure 10, in the case of a 200 RPM valve velocity the acceleration-like signal, recording a, which is given by the piezo element, is very sensitive to each event which the whole CVG installation undergoes. On this signal, the resulting shock of the flow cut-off at the valve, the cavity explosive growth in the test section, the shock of the valve opening, and the resulting water hammer of the cavity collapse at the valve level are visible during the first 20 ms of the signal. The corresponding pressure signal, recording b of figure 10, indicates the static pressure decrease to the vapour pressure according to the calculations of Figure 7. The Cranz-Schardin photograph sequence of Figure 11 shows the explosive growth of the vortex cavity, and corresponds to a 7 ms time delay from the start of the valve closing and a spark period of 200 ns. First, the liquid is ruptured in the

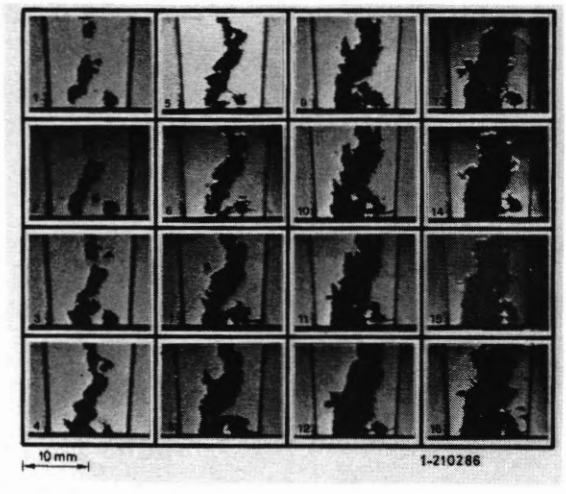

Fig. 11. Explosive growth of the cavitation vortex. Spark period : 200 µs, time delay = 7 ms. Exposure time : 300 ns, nominal flow rate 3.0 m^3/hour, N = 203 RPM.

form of individual cavities along the vortex axis. When all these cavities are gathered to fill the vortex core, the cavitation extends radially to the whole region of the pressure drop with a 1.7 m/s mean radial velocity of the cavity wall motion. The outward motion of the cavitation vortex is inverted when the incoming flow from the valve arrives in the test section. This happens when the cavity resorption in the valve is completed, see Figure 10. The resulting shock of this resorption is well visible on the acceleration signal 2.6 ms later than the start of the valve opening.

It takes 6 ms for the cavitation to disappear from the test section and the outlet pipe. Thereafter, a strong shock and a high pressure peak are detected by the two transducers. These correspond to the cavitation vortex collapse which is immediately followed by a cavity rebound. Hence, successive pressure wave series occur in the outlet pipe, between the downstream vessel and the test

section, leading to a new liquid rupture in the vortex core. A weak cavity collapse follows 6 ms later, as in the case of the previous collapse. This periodic phenomenon, which is driven by a mass oscillation, is rapidly damped, the pseudo-period being increased from 14 ms to 18 ms. Nevertheless, the strongest collapse, which causes the material damage of the test specimen, is the first occuring after the valve opening.

Cavitation vortex collapse. Due to the short time constants involved, both the piezo element and the pressure transducer are unable to track the cavitation vortex collapse dynamics. The Cranz-Schardin visualizations allow us to follow the cavity wall motion and the resulting pressure waves as long as the sequence of the 16 frames fall in the collapse time-history of interest. Hence, the frame rate increase of the camera is limited by the random time variation of about 100 ns between the trigger signal given by the start of the valve closing and the cavity collapse.

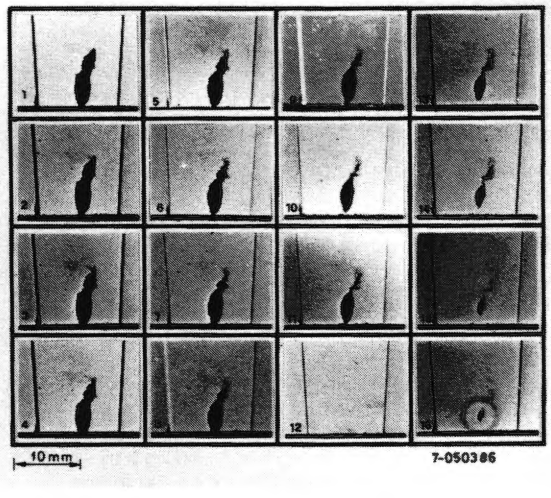

Fig. 12. Final stage of the cavitation vortex collapse. Spark period : 5 µs, time delay : 24 ms, exposure time : 300 ns, nominal flow rate : 3.0 m^3/hour, N = 203 RPM.

Two typical frame sequences are presented in Figure 12 and 13. Both of them are taken with a 24 ms time delay from the valve closing. The sequence of Figure 12 corresponds to the final stage of the cavity collapse, with a frame period of 5 µs. First an axial motion of the top of the cavity can be seen. The radial motion become significant as of the 9th frame. Due to this radial motion the tip of the cavity moves from the test specimen wall to the collapse center which is located at a height of 2 mm from the wall. The collapse takes place between

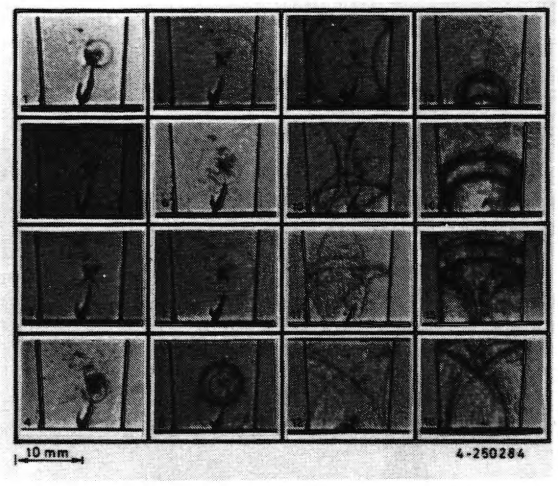

Fig. 13. Final stage of the cavitation vortex collapse followed by spherical shockwaves, spark period : 3 µs, time delay : 2.4 ms, exposure time : 300 ns, nominal flow rate : 3.0 m^3/h, N = 203 RPM.

the 15th and the 16th frame, and the spherical shock wave which results from the cavity rebound, is visible on the last frame. After the image reconstruction of the photograph we can follow the actual wall motion of the cavity by quoting the length and the radius of the cavity with respect to the time, see Figure 14.

The wall motion has a constant acceleration up to the ultimate stage of the collapse, which falls between the last two frames. The axial and radial mean acceleration values are 2.4 m/s^2 and 0.98 m/s^2, respectively.

To be able to calculate the collapse pressure, the time of the collapse has to be estimated. First, if we assume a constant acceleration for both the axial and radial motions, the cavity should vanish 2.4 µs or 4.4 µs later than the 15th frame, depending on what motion we follow. The mean time of 3.4 µs gives a mean rebound velocity of 690 m/s for the axial motion and 375 m/s for the radial motion. Moreover, by measuring the shock wave radius, the mean celerity value of the shock wave is estimated to 1660 m/s. In that case, the relations of the normal shock-wave lead to an overpressure of 6.2 kbar to 11.4 kbar through the shock front. However, the assumption of a constant acceleration could lead to an over-estimation of the time of the collapse and consequently increase the overpressure value. In order to estimate the time of the collapse, we can assume the same acceleration during the inward and the outward motion, this gives a collapse time of 3.2 µs and 2.8µs for the axial and the radial motion, respectively. The mean time of 3 µs leads to a mean rebound velocity of

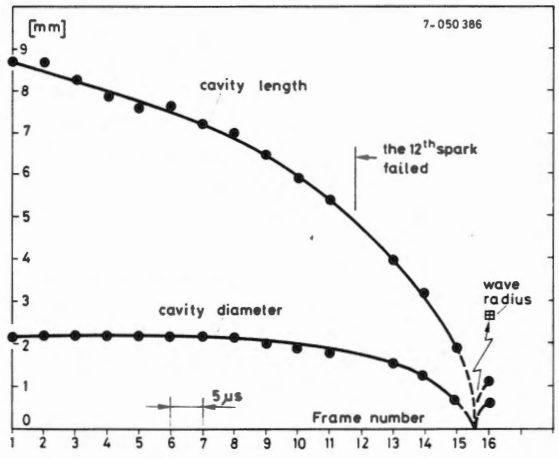

Fig. 14. The cavity height and diameter time history of the sequence of the Figure 11.

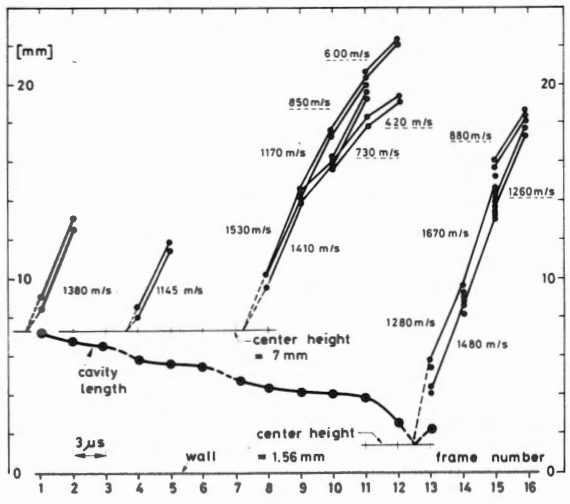

Fig. 15 Time evolution of the main cavity length of the Figure 13 and the corresponding shock waves radii added to their respective radiation center The reflected wave speeds are underlined.

550 m/s and 300 m/s for the both motions, respectively, and to a wave celerity of 890 m/s. The low value of the wave celerity is an indication that this assumption obviously is an underestimation of the collapse time. If we calculate a collapse time by using a wave celerity equal to the speed of sound, we obtain a time of 3.2 µs,which corresponds to rebound velocities of 610 m/s and 330 m/s overpressure values of 5 kbar to 9 kbar. In order to obtain the time of the collapse we can assume a constant acceleration motion, even during the ultimate collapse stage.

The sequence of Figure 12 is taken with a frame period of 3 µs in order to follow the waves' evolution and their interaction with the cavity.

In that case the break-up of the cavity core into several individual cavities produces successive collapses and the corresponding emitted shock waves. In spite of the irregularities of the cavities, the shock waves have a spherical symmetry. Moreover, these waves seem to be weak enough not to alter the motion of the main cavity which is attached to the wall.

These photographs have been reconstructed in order to compensate the optical distorsions and to get a 1.5% accurate measurement of the shock waves radii. In Figure 15, the radius of each visible wave is added to the height of their respective radiative center. The reflected waves are included and their celerity is underlined. Surprisingly they have very low wave celerity in contrast to the early stage of the direct waves. Nevertheless, celerity computations of the direct waves give values close to the theoretical speed value of the sound in pure water which is 1480 m/s.

In the case of the main cavity collapse, the cavity length decreases with a constant acceleration of - 0.95 m/s^2 except for the time between the 2nd and 3rd frames and the 6th and 7th frames which correspond to the collapse of a neighbouring cavity. The ultimate stage of the main cavity collapse occurs between the 12th and the 13th frame close to the test specimen wall at a height of 1.56 m. The collapse, resulting in spherical shock waves, and the rebound of the cavity are well visible after the 13th frame. A time of 1.8 µs later the 12th frame leads to a mean velocity of the cavity rebound of 690 m/s and a mean wave celerity of 3300 m/s, giving a 22.7 kbar overpressure through the shock wave. In addition the previous wave celerity value gives a Mach number of 2.23. By using the Tait equation of state for water, it is then possible to calculate the shock front overpressure if we neglect the flow velocity in front of the shock wave. In this case the calculations result in an overpressure of up to 32.6 kbar which is obviously different from the result obtained by the shock wave relations. The constant acceleration leads to an overestimation of the collapse time.

Moreover, if we made the assumption of an identical motion between the inward motion of the collapse and the outward motion of the cavity rebound, this leads us to a new collapse time of 1.7 µs which gives a mean velocity of 640 m/s and a mean wave celerity of 3050 m/s, giving a 19.5 kbar overpressure. The corresponding Mach number of 2.06 gives an overpressure of 25.7 kbars,which is closer to the value of 19.5 kbar already obtained by the relations of the normal shock waves.

Owing to the shorter frame period of that sequence, and in contrast to the previous sequence, this last assumption allows us to have a good pressure estimate. Nevertheless, in both cases we find pressure values of the shock waves, 6.2 kbars to 9 kbars in the first case and 19.5 kbar to 25.7 kbar in the last case which agree with the fact that cavitation can cause the plastic deformation and the subsequent erosion of any industrial alloy, even stellite. One exemple of the crater caused by a cavitation vortex collapse on 9060 stellite placed in the CVG is shown in Figure 16.

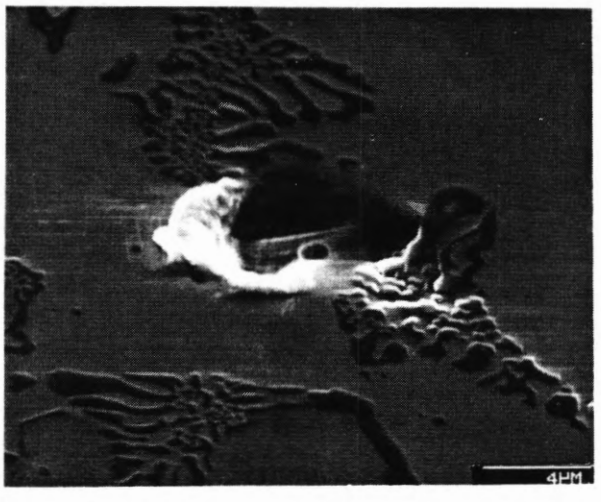

Fig. 16. Exemple of a crater produced on stellite in the cavitation vortex generator.

CONCLUSION

The cavitation vortex generator allows us to have an insight into the realistic cavitation erosion process of the industrial machines.

The simultaneous use of a pressure and a schock transducer and a high-speed vizualisations does not provide any evidence of interface instabilities which could generate microjets in contrast to the bubble cavitation collapse. But, in spite of the irregularity of the cavitation vortex, strong spherical shock waves are generated by the cavity rebound following the collapse. Estimations of the overpressure for these shock waves give values in the range of 6.2 kbar to 9 kbar in one case and 19.5 kbar to 25.7 kbar in the other presented case.

Therefore, these overpressure levels are high enough to explain the erosion of every industrial alloys in the hydraulic field.

ACKNOWLEDGEMENT

The authors wish to acknowledge all their colleagues from the EPFL cavitation group. They especially thank M. Farhat who carried out the Cranz-Schardin image data reduction and M. Maamouri for his help in taking the high speed photographs.

This research is financially supported by the Swiss Federal "Commission d'Encouragement à la Recherche Scientifique", The Swiss Energy producers association "Nationaler Energie Forschung Fonds", The Sulzer Brothers company and the Vevey Engineering Works company.

REFERENCES

1. Avellan, F. and Henry, P., 1987 Proc. EPRI Power Plant Pumps Symposium, ed. Electric Power Research Institute, New Orleans, March 1987, pp. 1 - 22.

2. Henry, P., Proc. Int. Conf. on Hydropower, Water Power 85, Las Vegas, vol. 2, pp. 1258-1267.

3. Avellan, F., Henry, P. and Ryhming, I., 1987, Proc. ASME Int. Winter annual meeting, Boston, dec. 1986, pp. 1-25, to be published.

4. Hinze, J.O., 1975, "Turbulence", 2nd ed. Mc Graw Hill, New York, pp. 600 - 614.

5. Lecoffre, Y., Marcoz, J. and Valibouse, B., 1981. Proc. ASME Fluids Engineering Conference, Boulder, June 1981, pp.

6. Karimi, A. and Avellan, F., 1986, WEAR, ed. Elsevier, vol. 113, no 3, pp. 305-322, December 1986.

7. Lamb, H., 1932, "Hydrodynamics", Cambridge University Press, Art. 145.

8. Henchoz, A., 1978. Proc. of Conference on High-speed Photography and Photonics, Tokyo, August 1978.